Evolution of thermal crystal zonations and their heterogeneity in crystal populations during magma cooling

C. Culha[1], T. Keller[2], J. Suckale[1]

[1]Stanford University, Department of Geophysics, 397 Panama Mall, Stanford CA 94305, USA.
[2]University of Glasgow, School of Earth and Geographical Sciences, 8NN University Avenue, Glasgow G12 8QQ, UK.

Key Points:

- Collective crystal settling in the form of clusters can lead to crystal zonations.
- Crystal clusters have lower than ambient temperatures and are hence zones where crystals preferentially nucleate and grow.
- Force chains tend to form within crystal clusters even at relatively low overall crystallinity.

Corresponding author: Cansu Culha, `cculha@stanford.edu`

Abstract

Crystal zonations provide valuable snapshot of the dynamic changes within a magma reservoir. However, there can be inconsistencies between crystals and their zonations, such that deciphering their signatures becomes convoluted. Crystals grow and shrink with temperature, pressure, and composition changes, which can change spatially and temporally as crystals transverse and evolve in the volcanic plumbing system. In this manuscript, we investigate how and at what spatial and temporal scales zonations record cooling processes in a magma lens after injection of fresh magma from depth. We simulate the cooling interface in either hot basaltic or dacitic magmas after their injection into a cold magma reservoir. We couple fluid dynamics to thermodynamics by allowing crystals with constant density and size to form and dissolve based on ambient melt properties and we resolve flow at the scale of each individual crystal. We infer zonations in our simulated crystals by tracking the temperatures they sample over time, but we do not grow or partially dissolve crystals. Our results show that when thermodynamics and fluid dynamics are coupled, a self-sustaining instability arises, because crystals transport the cooler-than-ambient melt in which they formed, creating conditions favorable to crystal formations where the crystal fraction is already high. Our results show that oscillatory zonation patterns can result from the self-sustaining instability, potentially overprinting larger, system-scale trends. Also, our results show that many of the crystals in the instability dissolve and lose their record of the instability. Many of the crystals that persist to the end of the simulation are shorter lived than the entire simulations, under estimating how long the domain remained at high temperatures. Our results suggest that zonations and their heterogeneity can be indicative of local instead of system scale processes, highlighting the importance of having multiple indicators to decipher a system scale process. Thus, we propose multiple indicators for the self-sustaining instability that we describe here.

Plain Language Summary

Similar to tree rings, crystals tell a story of their past through their zonations. However, unlike trees who are stationary and are constantly growing, crystals are dynamic and can grow as well as shrink. In order to understand what zonation patterns a natural sample crystal would record during a ubiquitous process, cooling, we built a simulator that is at the size of individuals crystals. We simulate the physics between crystals and melt, as well as, magma property change with temperature. Our results show that cooling a magmatic injection in a cold magma reservoir that forms denser than melt crystals can drive magma flow, which we call an instability. Since the simulator simulates each crystal, we can record the temperatures that a crystal samples over time, giving us insight into the zonations seen in natural sample crystals. Our results show that each crystal has a unique zonation that is dependent on the temperature distribution within its vicinity. Additionally, most of the crystals dissolve in the instability, so we lose their record. Overall, the crystals in our simulation can reproduce the confusing patterns that are often found in natural samples, suggesting that zonations are ubiquitous and deceiving. This highlights the importance of using multiple indicators to understand a process at the scale of the volcano.

1 Introduction

Some volcanoes erupt with little or no clear warning, raising questions about what processes in the plumbing system trigger eruptions. Individual crystals in erupted samples may contain vital clues, because they tend to exhibit zonations indicative of changes that occurred prior to eruption. These zonations manifest as variations in the chemical content along 1D profiles measured from crystal core to rim, or crystal profiles. Crystals grow or dissolve as a function of temperature (T), composition (C), and pressure (P) to re-establish thermodynamic equilibrium with their surrounding magma, preserv-

ing a tabular history of the conditions in the volcanic plumbing systems over time (Ginibre et al., 2007; Cashman & Blundy, 2013; Wallace & Bergantz, 2005). Hence, crystal profiles hold clues about the inner structure and dynamic changes within a volcano (Vance, 1962; Ginibre et al., 2007; Cashman & Blundy, 2013; Wallace & Bergantz, 2005), but deciphering these clues has proven challenging.

At a large scale, temperature, composition and pressure appear to be approximately homogeneous in many volcanic systems (Flynn & Mouginis-Mark, 1994; Whitney & Stormer, 1985; Bachmann et al., 2002). At the crystalline scale, individual crystals paint a different picture. There is significant heterogeneity in the zonations of individual crystals. Even within a given sample, neighboring crystals may exhibit different zonations (Wallace & Bergantz, 2005; Bachmann et al., 2002). Our aim is to recognise the coherent story recorded by the heterogeneous crystal record.

Analyses of isotopic, trace, and chemical signatures along crystal profiles is advancing our ability to dissociate the different contributions (T, P, fO_2 and Comp.) that result in zonations (Cashman & Blundy, 2013; Cooper, 2019; Costa et al., 2020). Of these contributions, variability in temperature, or thermal zonations, has attracted particular attention as they may be related to eruption triggering mechanisms. Some studies have argued that thermal zonations suggest that mafic injections into magma reservoirs may trigger eruptions (e.g. Cashman & Blundy, 2013; Murphy et al., 2000; Bachmann et al., 2002; Shane & Smith, 2013); while other studies suggest that thermal zonations indicate latent heat release due to decompression crystallization (Blundy et al., 2006) or large scale thermal convection (e.g. Singer et al., 1995).

Many crystals in igneous rock samples show thermal zonations that evidence thermal changes in their host magma over time, but not all neighboring crystals show the same thermal zonations. The heterogeneity in crystal populations indicates thermal variability over small spatial scales. Thermal convection was one of the first hypotheses proposed to explain crystal heterogeneity (e.g. Singer et al., 1995; Bachmann et al., 2002; Huber et al., 2009; Murphy et al., 2000), but it requires large magmatic bodies or low viscosities to sustain convection. Although plausible, recent studies of plutons highlight that melt-rich magma bodies likely exist as ephemeral, thin lenses within a larger crystal-rich mush zone. Another explanation is magma mixing (Sparks et al., 1977; Davidson & Tepley, 1997; Zellmer et al., 2003), a hypothesis that is consistent with geologic examples of magma mingling like enclave and schlieren formations (e.g., Alasino et al., 2019; Barbey et al., 2008), but limited in explaining the speed of chemical mixing (e.g. Till et al., 2015; Rae et al., 2016).

While thermal zonations have been studied a lot in more felsic and hence more explosive systems, thermal zonations also form in milder, more mafic eruptions. Volcanic sites like Hawaii and Stromboli are consistently erupting mafic magmas that can be traced back to a homogeneous parent magma sourced from the mantle (e.g., Murata, 1970; Dupuy et al., 1981; Treiman, 1997). Even in these eruptions, heterogeneous thermal zonations in neighboring olivine and plagioclase crystal populations are well preserved (Kahl et al., 2011; Ruth et al., 2018), indicating that thermal zonations and heterogeneity at the crystalline scale are common signatures in many volcanic systems.

In our previous work (Culha et al., 2020), we simulate dense crystals unstably stratified in melt-rich magma. We observe crystals collectively settling naturally creating a small scale flow. We hypothesize that small-scale flow within melt-rich magma lenses will result in complex thermal zonations in individual crystals as well as thermal zonation heterogeneity in the crystal population. In order to test our hypothesis, we deploy a similar numerical model to our previous work to capture the same hydrodynamic interactions between crystals and melt at low crystal volume fraction. We introduce a coupled model of thermal evolution, crystallization, and crystal remelting. We couple thermal evolution with phase-change reactions and fluid mechanics, the collective we call magma

dynamics, by considering a magma of constant bulk composition but varying crystallinity, melt density, and viscosity as constrained by thermodynamic phase equilibria modeled with rhyolite-MELTS (Gualda et al., 2012; Ghiorso & Gualda, 2015). The model setup represents a hot, low-crystallinity, low-viscosity magma injected into a cool magma mush reservoir. Crystals forming near the cooling interface are expected to settle collectively in clusters, thereby sustaining crystal-driving overturn flow and convective cooling of the layer, which we call a self-sustaining, crystal-driven instability.

In our simulations of the self-sustaining instability, we observe individual crystals sampling complex and locally heterogeneous thermal histories, suggesting that local-scale dynamics can create unique crystal zonations even for crystals involved in mesoscale collective flow patterns. Furthermore, systematic coupling between fluid mechanics and phase-change reaction leads to preservation bias of crystals only from certain flow histories. This result suggests that local-scale heterogeneity can overprint broader system-scale trends, highlighting the challenges of deducing system-scale dynamics from individual crystal records. In light of this result, we propose multiple indicators that in combination will allow better interpretation of magma dynamics from thermal zonation profiles.

2 Methods

To better understand the coupled thermal evolution and crystal-riven magma dynamics we formulate a model of a hot, melt-rich lens cooling after injection into a cooler mush body (Fig. 1A). To derive testable model predictions at the scale of individual crystals, we use a direct numerical simulation technique to resolve the formation of crystals near the cooling interface and their segregation into the adjacent melt-rich layer.

Our model is based on solving thermally coupled Stokes flow with crystals resolved as rigid bodies and their hydrodynamic interactions with surrounding melt. To maintain a crystallinity at equilibrium with the thermal evolution, we use a crystal population control algorithm that counts crystals present in a control volume of ten times the crystal diameter and adds/removes crystals to keep crystallinity close to the equilibrium value (Fig. 1B). To capture small changes in crystallinity (Fig. 1C,F) yet resolve the dynamic subtleties in the domain arising from spatial variations in melt density and viscosity (Fig. 1D-E and G-H), we choose a control volume size that is 10 times larger than the crystal radius in both the lateral and vertical direction. This grid setup enables us to capture crystallinity differences of $\sim 2\%$. Below, we first describe the cell scale flow dynamics model and then we describe how we set a thermodynamic equilibrium at the control volume scale by adjusting crystallinity of the simulation.

We solve for conservation of mass, momentum, and energy in a crystal-bearing, incompressible melt. Due to the high viscosity of the magma, inertial effects are negligible, reducing momentum conservation to the Stokes equation. We model both basaltic and dacitic magma (Table 1; Browne et al., 2006) as representative compositions, Fig. 1C–E and F–H, respectively, to highlight that our approach can be generalized to different compositions of melt-rich systems. For simplicity, we ignore latent heat of crystallization.

The governing equations for the melt phase are incomprehensibility, Stokes and energy conservation,

$$\nabla \cdot \mathbf{v}_\ell = 0 \tag{1}$$

$$0 = -\nabla P + \nabla \cdot (\mu_\ell \nabla \mathbf{v}_\ell) + \rho_\ell \mathbf{g} + \mathbf{F}_c \tag{2}$$

$$\rho c_p \left(\frac{\partial T}{\partial t} + \mathbf{v} \cdot \nabla T \right) = \nabla \cdot \left(k \nabla T \right) \tag{3}$$

where t is time, $\mathbf{v}_\ell$ is the velocity of the melt, μ_ℓ is the melt viscosity, ρ_ℓ is the melt density, P is the melt pressure, $\mathbf{g}$ is gravity, $\mathbf{F_c}$ is the force exerted by the crystals on the

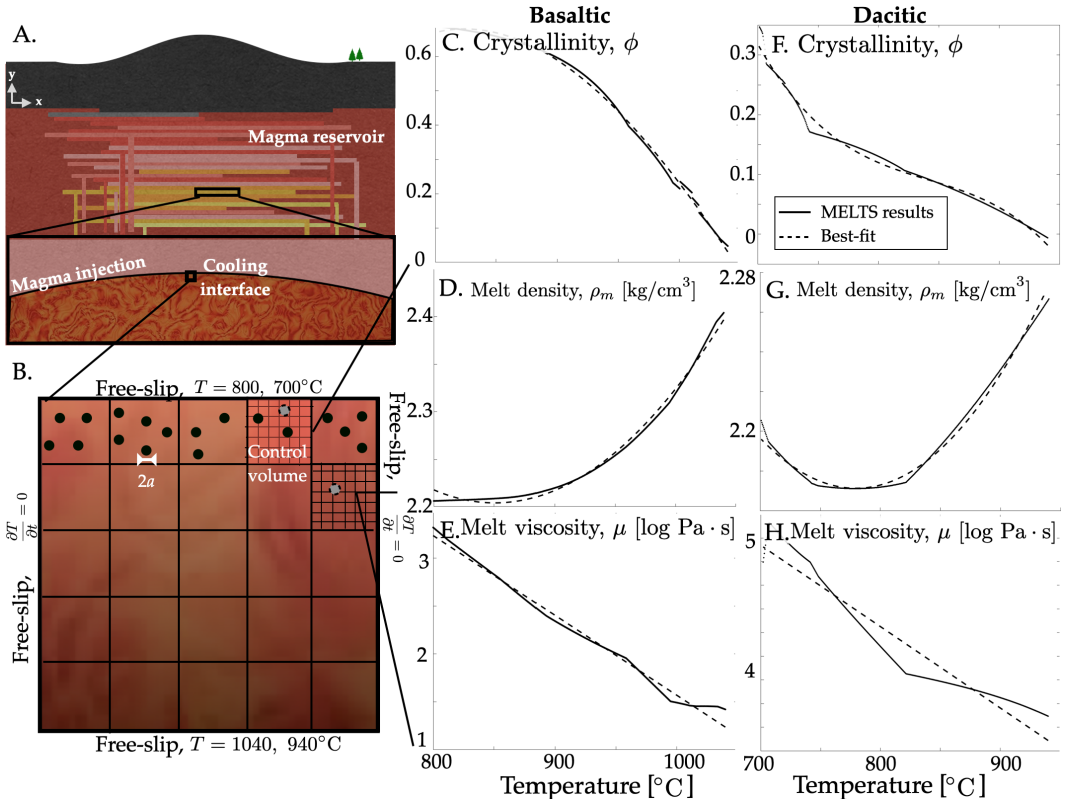

Figure 1. rhyolite-MELTS results. We zoom into the cooling interface of a magma injection within a magma reservoir (A). We use basaltic and dacitic compositions to model phase equilibria for a range of temperatures at constant pressure to specify crystallinity (C and F), melt density (D and G) and melt viscosity (E and H) using the rhyolite-MELTS software. We update the crystallinity in a control volume of several grid cells by adding/removing crystals to match the calculated equilibrium, whereas we update the melt viscosity and density to their equilibrium value within individual grid cell (B). We use a different temperature range for basaltic composition from dacitic composition.

liquid, c_p is the heat capacity, and k the heat conductivity. We take the heat capacity of melt and crystal phases to be the same. The boundaries as shown in Fig. 1B are free slip, $\frac{\partial \mathbf{v}}{\partial \mathbf{n}} = 0$, where $\mathbf{n}$ is the vector normal to the boundary. The top and bottom temperatures of the domain are isothermal for basaltic and dacitic compositions (values given by Browne et al. (2006)). The left and right walls are set to insulating $\frac{\partial T}{\partial t} = 0$. We set the initial temperature profile as,

$$T(y, \tilde{t} = 750s) = \frac{(T_t + T_b)}{2} - \frac{(T_b - T_t)}{2} \mathrm{erf} \frac{(y - H)}{2\sqrt{D_T \tilde{t}}} \tag{4}$$

where T_t and T_b are the initial top and bottom boundary temperatures, erf indicates the error function, H is the domain height, y is the vertical coordinate with initial uniformity in the x direction, and $D_T = k/\rho c_p$ is the thermal diffusion coefficient. We model only after heat has been lost diffusively for a time period $\tilde{t}$, an initial interval that would be nearly crystal-free and therefore without significant flow dynamics.

We assume that the crystal-free melt is Newtonian such that all non-linear effects apart from thermodynamics coupling are a consequence of the coupled multiphase dynamics. The governing equations for the crystal phase are Newton's equations of rigid-body motion

$$M_c \frac{d\mathbf{v}_c}{dt} = \mathbf{F}_c + M_c \mathbf{g} \tag{5}$$

$$\frac{d\left(\mathbf{I}_c \cdot \omega_c\right)}{dt} = \mathbf{T}_c \tag{6}$$

$$\frac{d\mathbf{X}_c}{dt} = \mathbf{v}_c \tag{7}$$

where M_c is the mass of an individual crystal, X_c is the crystal position at center of mass, $\mathbf{v_c}$ is the velocity of a crystal at center of mass, ω_c is the angular velocity of the crystal, $\mathbf{F}_c$ is the hydrodynamic force on crystals, $\mathbf{T}_c$ is the crystal torque resulting from the surrounding melt, and $\mathbf{I}_c$ is the moment of inertia tensor of a crystal.

For simplicity, we consider only a single type of crystal that is denser than the melt phase and has a constant radius, $a = 0.1$ cm. We set the crystal density to be a typical olivine crystal density (3000kg/m^3) in the basaltic simulations and feldspar crystal density (2600kg/m^3) in the dacitic simulations. The crystals conserve momentum at the wall boundary, but the high viscosity slows the crystals such that the crystals do not get into direct contact with the walls or with one another. To resolve the long-range hydrodynamic interactions between crystalline and melt phases, we use a customized, multiphase solver for magmatic systems that has been extensively bench-marked in previous studies (Suckale et al., 2012a; Qin & Suckale, 2016, 2017; Qin et al., 2019).

We use the thermodynamics model rhyolite-MELTS (Gualda et al., 2012; Ghiorso & Gualda, 2015) to obtain equilibrium phase proportions, melt density, melt viscosity, and the evolution of magma and crystal compositions with temperature for a given magma bulk composition (Table 1), pressure (200 MPa) and initial oxygen fugacity (Nickel-nickel oxide). We do not impose a fixed oxygen fugacity buffer for equilibrium calculation at different temperatures because there is no substantial evidence suggesting magma cools along a buffer (e.g. Borisov & Behrens, 2013; Borisov, 2016; O'Neill et al., 2006; Sack et al., 1980; Kress & Carmichael, 1991; Jayasuriya et al., 2004). In Fig. 1, we show the change in crystallinity (ϕ), melt density (ρ_m), and dynamic viscosity (μ) for each given magma composition as a function of temperature (T) together with best-fit polynomials which we use to more efficiently access equilibrium calculations in our flow-dynamics simulations.

We keep the bulk composition of the magma to be constant, such that we are not considering compositional effects in this model. We approximate the melt composition

Table 1. We base our compositions on the average compositions sampled by the Unzen eruption described in Browne et al. (2006). To estimate the basaltic composition, we use the mafic enclave composition. We created a line of best fit for each chemical content relative to SiO_2 content for the mafic enclave and the host magma. We use the reported SiO_2 content for the estimated basaltic and dacitic magma compositions Browne et al. (2006)and calculate the chemical compositions from the best fit. Then we normalize the compositions. The reported dacitic composition is the average composition.

Comp.	SiO_2	TiO_2	Al_2O_3	Fe_2O_3	MnO	MgO	CaO	Na_2O	K_2O	P_2O_5	H_2O	T range
Basalt	48.83	1.21	18.07	9.62	0.17	5.14	9.25	2.65	0.94	0.22	3.91	800-1040°C
Dacite	57.33	1.01	17.04	7.02	0.12	3.33	6.88	3.33	1.74	0.18		700-940°C

change as a function of temperature by varying density and viscosity as a function of temperature at the cell scale. However, the system is dynamic and crystals disturb the thermodynamic equilibrium as they advect through the domain. We take the average temperature and crystallinity over all of the cells in a control volume and compare to the equilibrium crystallinity at the given control volume temperature as given by rhyolite-MELTS (Fig. 1C–H). To enforce thermodynamic equilibrium, crystals are added or removed until the crystallinity is within less than one crystal per control volume of the equilibrium value. We call crystal removal and addition as "dissolution" and "formation" in the manuscript, respectively. For numerical stability reasons, there is a 2 crystal size buffer region near the walls where crystals do not form.

3 Flow dynamics coupled to thermal evolution and phase change results in a self-sustaining convective instability

To identify the dynamic coupling between reactive changes in crystallinity and flow dynamics, we compare two simulations at basaltic bulk composition in Fig. 2. In one of the simulations equilibrium crystallinity is maintained by crystal population control during dynamic flow (Fig. 2A-C). In the other, equilibration by phase change is neglected and instead a constant number of crystals is maintained over time (Fig. 2D-F). The latter simulation consistently assumes a constant melt density of 2200 kg/m^3 and melt viscosity of 95 Pas. The former simulation has melt density vary from $2200-2450$ kg/m^3 and viscosity from $95 - -10^3$ Pa·s (Fig. 1D-E).

The crystals in both simulations settle under the joint influence of gravity and the hydrodynamic forces arising from the presence of other crystals. The hydrodynamic interactions are important dynamically because they break the otherwise linear symmetry of Stokes flow, leading to spatially heterogeneous crystal clusters (Culha et al., 2020). As a consequence, the crystals in both simulations form a cluster that sinks to the bottom of the domain (Culha et al., 2020). While in both simulations the initially present crystals drag cold magma along as they settle collectively, only in the simulation enforcing thermodynamic phase equilibrium is the cooling boundary layer replenished with newly precipitated crystals. In the control simulation without equilibration, settling of a constant crystal population leaves behind a gap in crystal distribution along the boundary. The result of equilibration coupled to dynamic flow is that more crystals form in regions where an instability is already growing, thereby further enhancing the instability. Hence, the growth rate of the instability in the simulation including phase change is significantly faster than without it.

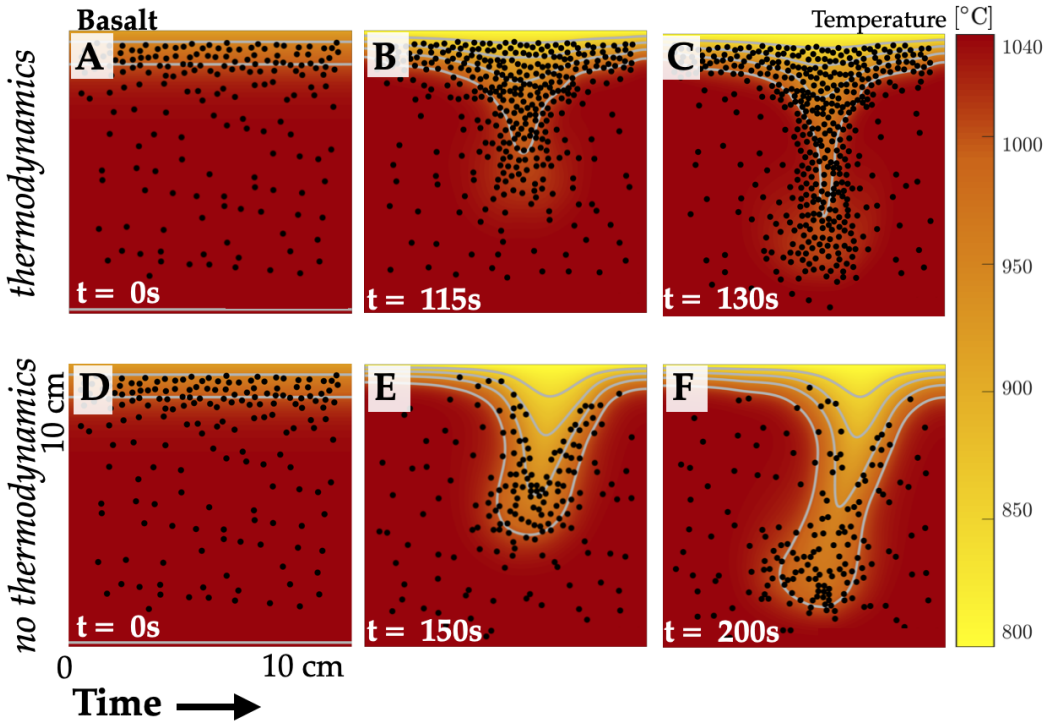

Figure 2. Coupling flow dynamics to thermal evolution and crystal precipitation/dissolution leads to a self-sustaining instability. We show 2 simulations, one maintaining equilibrium by crystal population control during dynamic flow (A-C) and one without equilibration, where melt density and viscosity are held constant and the initial number of crystals is left to evolve without precipitation/dissolution (D-F). Both simulations start with the same initial crystallinity and identical crystal positions.

The morphology of the two instabilities, as indicated by the gray temperature contour lines in Fig. 2, is significantly different. In the simulation that integrates thermodynamics, the temperature field exhibits a sharp tip reminiscent of a needle that protrudes and incubates the cooler magma into the hotter magma below. The formation and dissolution of crystals enhances and localizes the cold magma drip, forming a thin crystal rich spine that widens diffusively towards the tip. Although the cooler melt at the top of the domain has a higher melt viscosity, resisting flow, the continual diffusion and advection of temperature locally with crystal advection increases the crystal load and hence driving force. The propagation and growth of the instability hence accelerates, leading to a strongly heterogeneous distribution of crystals throughout the domain. The simulation that integrates thermodynamics hence forms an instability that grows quickly and is self-sustaining, unlike the instability in the simulation without thermodynamics.

Whereas the simulations shown so far both used a basaltic magma composition, we now wish to establish if the observed dynamics are robust for the second, dacitic reference composition as well. One of the pertinent differences between basalt and dacite is the melt viscosity (Fig. 1E,H). In Fig. 3, we compare snapshots of four simulations, two that include phase change equilibration (A-B) and two that neglect phase change but differ in melt viscosity by three orders of magnitude (C-D). To facilitate our analysis, we non-dimensionalize our results. We take the crystal radius, a, and the Stokes speed, $\Delta v_s = \frac{2\Delta\rho a^2 g}{9\mu}$, as the characteristic size and speed. At the same non-dimensional time, the two simulations without thermodynamic coupling result in an identical crystal distribution, suggesting that in the absence of thermodynamic effects, we expect crystal clusters to form in both basalt and dacite.

Fig. 3A shows the same snapshot as Fig. 2C from the simulation including equilibration by phase change for the basaltic composition. We compare this simulation to the evolution of crystallinity using a dacitic magma composition shown in Fig. 1 and Table 1. Dacitic magma crystals often record cooler temperature ranges than basaltic magmas; hence we model the thermodynamics at 700-940°C temperature range, while keeping the pressure the same as the basaltic run. At a similar non-dimensional time, basalt and dacite simulation show very different results (Fig. 3A-B). In the case of dacitic magma (Fig. 3B), the domain crystallizes in a spatially homogeneous way without forming a pronounced instability as in Fig. 3A. While this comparison does not mean that this instability is universally absent in dacitic compositions, it suggests that the relatively slow crystal settling speed does not keep pace with the diffusive growth of the thermal boundary layer, which suppresses the growth of the instability. Conditions amenable to instability formation in dacitic magma are more rare than in the basaltic context.

The differences between the thermodynamically coupled basaltic and dacitic simulations arise due to competing speeds: (a) crystal advection speed and (b) thermal diffusion speed, which determine if a crystal cluster instability forms in magmatic settings. We choose (a) the Stokes speed as the characteristic speed scale for the crystalline phase, and (b) the diffusive thermal front speed as a function of thermal diffusion and thermal diffusion length scale, $v_T = f(D_T, l_T)$. We refer to the ratio between the two speeds as K, where

$$\mathrm{K} = \frac{v_T}{\Delta v_s} = \sqrt{\frac{D_T}{\tilde{t}}}\frac{9\mu}{2a^2 g(\rho_c - \rho_m)}. \tag{8}$$

Low values of K represent conditions where the growth of a self-sustaining instability by crystal-driven advection is fast with respect to the diffusive growth of the cooling boundary layer as shown in Fig. 3A. At high values of K, the growth of the instability is suppressed by the comparatively rapid advance of thermal diffusion (Fig. 3B).

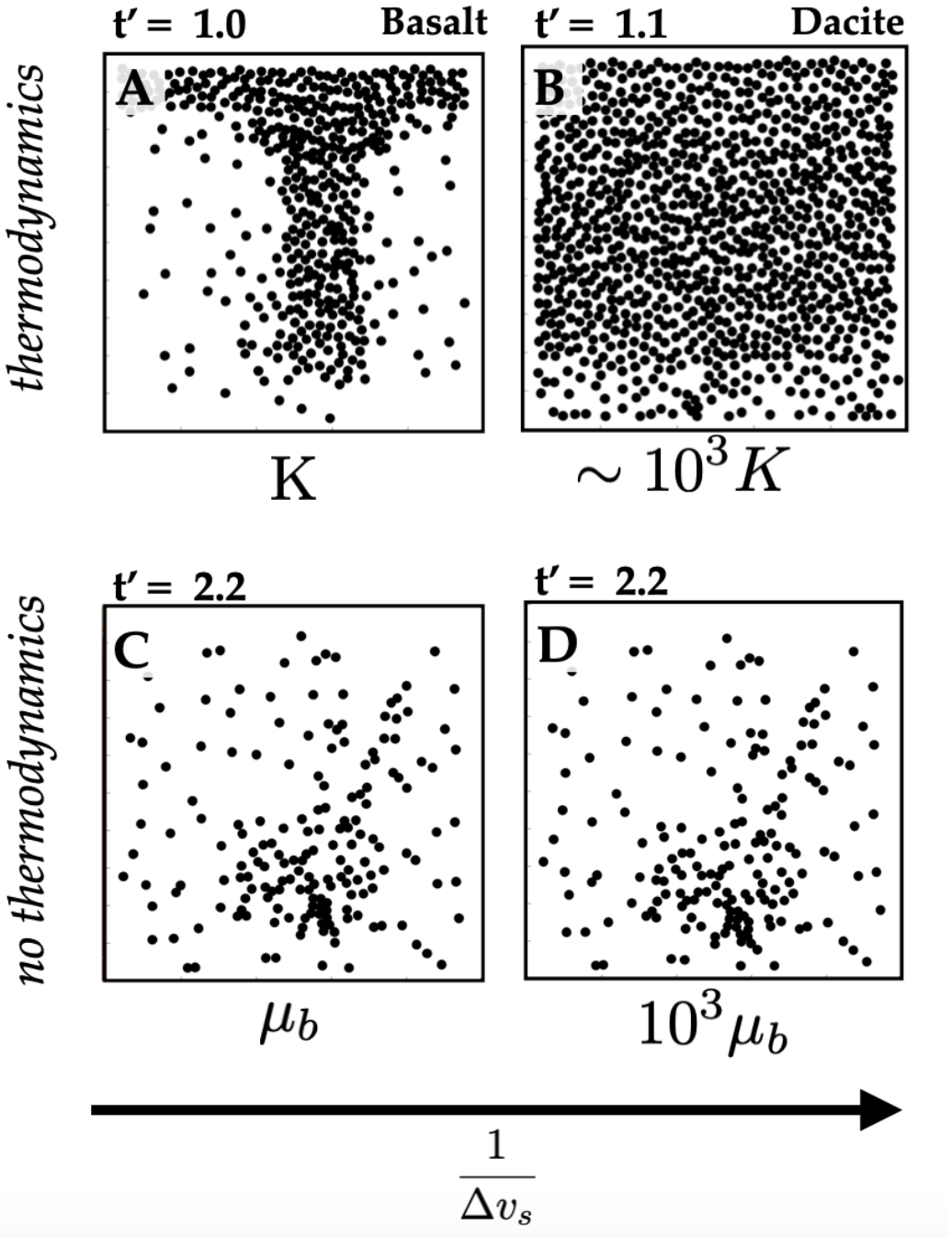

Figure 3. High K hinders the instability. Temporal snapshots of four simulations: two with (A-B), and two without phase change (C-D). Simulations A and C as well as B and D start with the same initial crystallinity. We only increase the viscosity in D from C. We present our results in non-dimensional form.

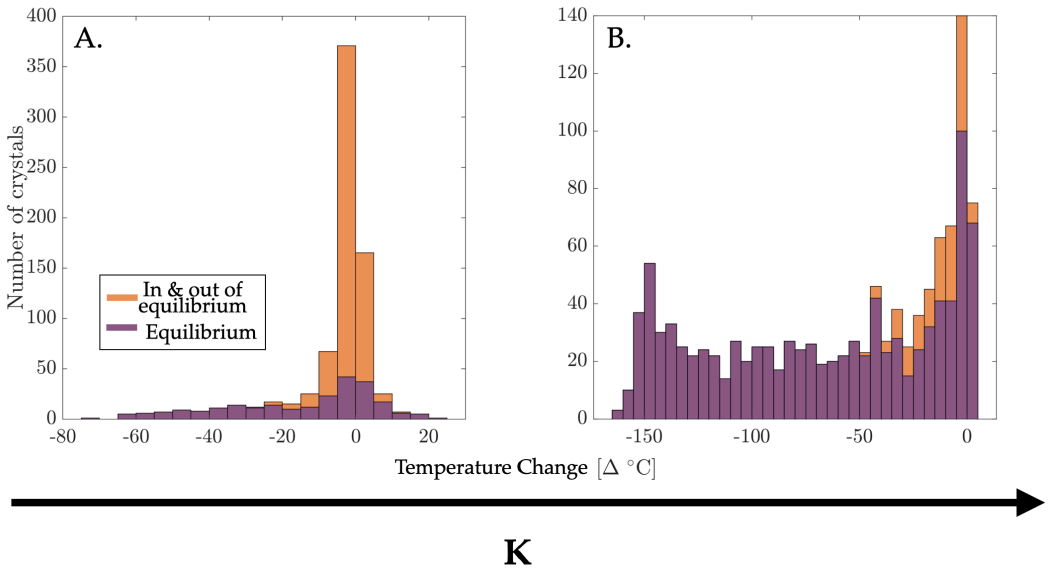

Figure 4. Temperature changes for crystals in and out of equilibrium Histogram of the temperature change between formation temperature and final crystal temperature for individual crystals during the two simulations in Fig. 3C-D. Histogram in A has crystals that formed throughout the simulation in Fig. 2A-C and C, whereas histogram in B has crystals that formed throughout the simulation in Fig. 3D. The purple histogram shows crystals that lasted to the end of the simulation snapshot in Fig. 3A-C and the orange histogram includes crystals that also dissolved during the simulation, "crystals out of equilibrium". For crystals that are out of equilibrium, the final crystal temperature is the temperature at which the crystal was last present.

4 Most crystals in self-sustaining crystal clusters dissolve

Crystals entrained in the established flow instability may become disequilibrated with evolving thermal conditions. In our simulations, we instantaneously dissolve a crystal that is "out of equilibrium" in, in the sense that it has moved into a control volume where the average crystallinity now exceeds the calculated equilibrium value. In natural samples, crystals that are out of equilibrium initially have their rims dissolved and, with time, might dissolve completely. In our simulations we can keep track of the thermal history of crystals regardless of whether they survived until the end of the simulation. We identify the temperature change of each of the crystals by recording its temperature at formation as well as the time of their dissolution (a) or the stopping time of the simulation (b). In many cases, the crystals oscillate in temperature, hence this metric is not necessarily representative of the maximum temperature range of a crystal history.

In Fig. 4 we show the temperature change each crystal experiences over a temperature range of 240°C, the initial maximum temperature contrast within the simulation. Fig. 4A and B correspond to the simulations in Fig. 3A and B, respectively. We only record crystals that last for at least two model output frames to compute a temperature difference. We show the crystals that last until the end of the simulation in purple and all of the crystals that existed for more than two model output frames throughout the simulation in orange.

In Fig. 4A, the two histograms for the low-K simulation are different: at least 69% of the crystals in Fig. 4A formed and/or dissolved during the simulation. In Fig. 4B, the two histograms for high-K simulation are similar: about 13% of the crystals in Fig. 4B dissolved during the simulation. Most crystals in the high-K value simulation stay in thermodynamic equilibrium, indicating that less dynamic disequilibration has occured in the absence of the flow instability. In comparison, Fig. 4A shows that most of the crystals in the self-sustaining crystal cluster are out of equilibrium and hence lose their ability to testify for the processes happening in the simulation. In natural samples, this likely translates to crystals exhibiting dissolved rims or perhaps completely dissolved crystals. Either scenario implies a partial or full loss of thermal history recorded in crystal zonations, which we discuss more in the next section.

5 Self-sustaining instability leads to thermal zonations

While both simulations in Figure 4 start with the same gradient in temperature of 240°C, 23% of the crystals in equilibrium predominantly show heating in Fig. 4A, whereas only 3% of the crystals in Fig. 4B show heating. Additionally, the crystals show a wide range of temperature changes. Natural crystal samples show evidence of heating as well as heterogeneity in zonations in crystal populations. In order to better assess whether this process can reconstruct the heating and cooling zonations observed in crystal populations as well as the zonation heterogeneity in crystal populations, we look at a simulation that lasts for a longer period of time than in Fig. 2-4. We run a thermodynamically coupled simulation that models magma properties of basalt on a domain that is three times the size of the simulation in Fig. 2A-C. While the initial condition of the simulation is the same as in Fig. 2A-C, the larger domain allows for two crystal cluster instabilities forming in parallel. We are able to capture instability interactions, which ultimately determine where and when crystals form and how crystals sample the magma dynamics. To best illustrate how crystals are migrating through the domain, we highlight different crystal sub-populations in color.

Two crystal cluster instabilities form in Fig. 5A-C. The one on the right advances relatively rapidly through the domain and the tip of the instability separates from the spine. These waves of instability detachment are rarefaction waves (Manga, 1996) that

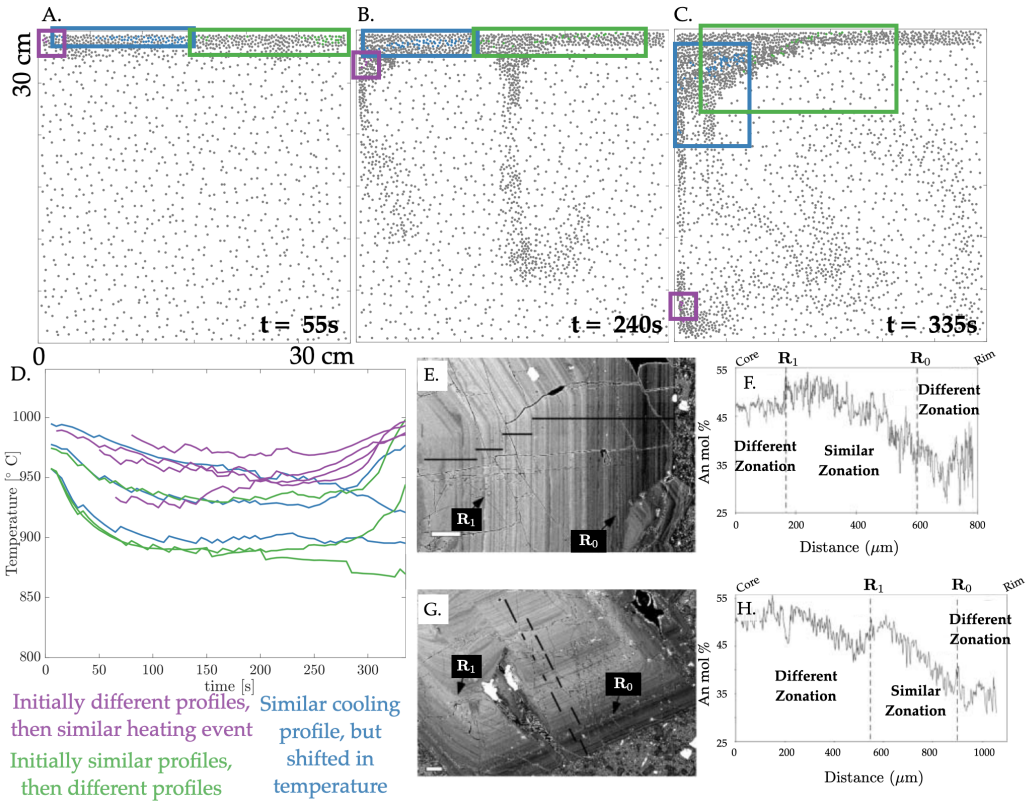

Figure 5. Crystal displacement on scales comparable to crystal diameter may result in crystal zonations unique from the crystals in their immediate vicinity A-C shows snapshots of a simulation with same initial conditions as the simulation in Fig. 2(A-C) but 3x the size of that in Fig. 2A-C. Three crystal sub-populations are highlighted to show how crystals move together in some regions and separate in others. Purple crystals are crystals that traveled to the bottom of the domain over the course of the simulation. Blue and green crystals formed in the left and right sides of the top domain, respectively, and remained in the top half of the domain during the portion of the dynamics shown here. The square box encapsulates all of the crystals in each category. D shows temperature profiles of crystals from A-C. We compare our results to natural samples from (Ginibre et al., 2002). The anorthite content zonations of E and G are in F and G.

arise as a consequence of the nonlinear dependence of crystal settling speed on crystal fraction. The right and left sides of the spine thermally pinch during this separation, which heats the tip of the spine that no longer has a cluster head. The heating of the spine tip as well as the cluster head dissolves many crystals, dampening the rarefaction wave while amplifying the nonlinear dynamics of the system. It appears as if the spine is retreating back to the cooling wall as the left cluster begins to advance down the domain, dominating the flow. At the initial stages of cluster formation, there is a distinct upwelling between the two clusters. However, as the clusters advance through the domain, the flow at the bottom of the domain from left to right begins to dominate, stalling the upwelling between the clusters. The result is a single large convection cell. As this flow dynamic evolves, the right cluster gets pushed to the left cluster.

We highlight 3 crystal sub-populations in purple, blue and green to demonstrate their differential movement with respect to each other in this dynamic system. Most crystals in these sub-populations escape dissolution for the majority of the simulation. Blue and green crystals form on the left and right sides of the domain, respectively, and remain within the top half of the domain over the course of the simulation. Purple crystals are a subgroup of the blue crystals; they reach the base of the domain first. The colored squares encapsulate all of the crystals in each of those sub-populations. The different sub-populations reveal that crystals that start near one another, such as purple and blue crystals, can end in very different parts of the domain due to the cluster dynamics. Conversely, crystals starting out in different segments of the domain can move closer to one another and even mix, such as the green and blue crystals.

Fig. 5D shows 3 randomly chosen detailed thermal crystal histories in each of the purple, blue and green sub-populations. We record the temperature of the cell that is closest to the crystal center over time to record these thermal histories. This choice is a simplification, since in natural samples each crystal zonation is thought to sample the temperature of the melt that the crystal is equilibrating with along its rim.

The green crystals form near the same temperature and cool similarly, but then their zonations change such that some of them begin to show significant heating while others show continued cooling. Consistent with the green crystals, the 3 blue crystals have similar cooling zonations, but they start at different initial temperatures and stay shifted in temperature while they experience similar degrees of heating and cooling. Finally, the purple crystals, which remain close to each other throughout the simulation, initially have different formation temperatures and degrees of cooling/heating, but as they advect with the cluster, they sample similar temperatures. These results show that crystals in immediate proximity to each other, as could be found in a field sample, could be part of the sample magma dynamics, while sometimes capturing different thermal zonations and other times capturing same thermal zonations.

In Fig. 5E-H, we compare our results to natural plagioclase samples from the Parinacota Volcano basaltic eruption in Chile (Ginibre et al., 2002). The study shows that strontium trace element and anorthite content show zonations along crystal profiles. In Fig. 5F and G, we reproduce the An content for the backscatter electron images of the two plagioclase crystals in Fig. 5E and G, respectively (Ginibre et al., 2002). The original work identifies two resorption zones, R_0 and R_1, that mark the termination and onset, respectively, of zonations in the plagioclase samples that appear to be similar to one another. In Fig. 6E-H, from the crystal core to R_1, the two crystals have different zonations to one another: the crystal in F shows little variance in anorthite content whereas the crystal in H shows a general decrease in anorthite content. Between R_1 and R_0 they both decrease in anorthite content to 35%, showing similar zonations. However, similar to their first zonation, the length of the zonation is different between the two crystals. Finally, after R_0 to the crystal rim, each of the crystals have a different degree of variability in anorthite content. The study argues that two basaltic magmas (one with high and another with low Sr and An content) differentiated and experienced turbulent

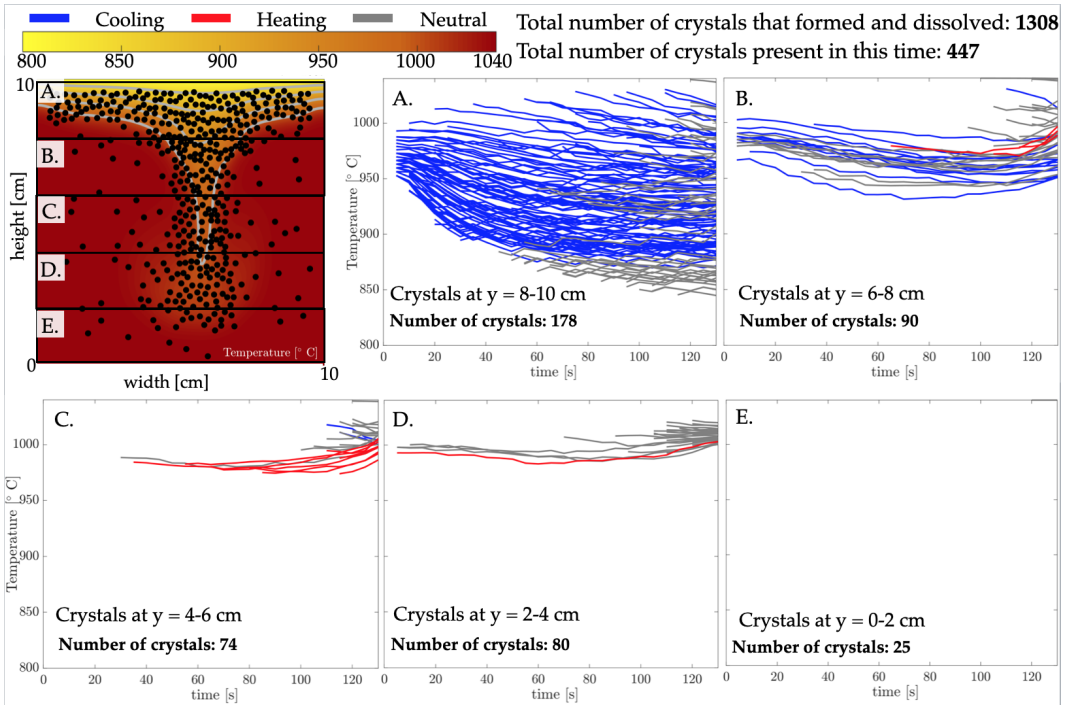

Figure 6. Bias in our crystal analysis. We show the final snapshot of the simulation in Fig. 2A-C. The instability is split into different segments and the crystal profiles of each section is shown in plots (A-E). The blue, gray and red profiles suggest that the crystal experienced overall cooling, less than 10°C temperature change, or heating, respectively.

mixing (Ginibre et al., 2002). Instead of invoking turbulence in a highly viscous magmatic system, we provide an alternative explanation rooted in the nonlinear dynamics of multi-phase flow.

Temperature plays a key role in anorthite and trace element concentrations, such that a change in 10s of degrees Celsius can alter anorthite content by a few percent (Cashman & Blundy, 2013; Santo, 2005; Kojitani & Akaogi, 1995). In Fig. 5D, we do not model crystal growth and we cannot run models on more realistic domain sizes that would allow for crystals to experience longer histories. Nevertheless, the thermal history zonations showcased here could be observable in the form of different growth zonations for crystals like plagioclase. As shown in Fig. 5, a crystal can initially have different zonations that then experience similar zonations (purple crystals) and similar zonations that then transition into different zonations (green crystals) from the crystals that are within their vicinity, similar to the crystals in Fig. 5E-H. Additionally, we do not allow crystals to stay in the simulation once dissolved, hence we are not be able to capture any gaps in the crystal history analogous to a dissolution rim. Including dissolution along a crystal profile would allow the simulated crystals to last longer and show more varied zonations.

6 Crystals provide an incomplete record of magma dynamics

Our analysis questions how well crystals testify to dynamically evolving conditions within a magmatic system. In Fig. 4, the orange histograms center around small temperature changes, whereas the purple histograms preserve a larger distribution of temperature changes. Our results suggest that the crystals who stay in equilibrium tell a dif-

ferent story than the crystal who have experienced disequilibration, inducing a bias in our crystal zonations analysis in Sec. 5. We specifically look at which parts of the dynamics the crystals sample and which parts they omit in their record of the instability. In Fig. 6 we split the instability into 5 segments and look at the temperatures the crystals sample with time in each of the segments leading up to the end of the simulation. If the crystal profile overall experiences heating, cooling or less than 10°C temperature change, then the profile is displayed in red, blue or gray, respectively.

Due to the cooling boundary with increased melt viscosity, some of the crystals at the top of the instability stay trapped and cool with time (Fig. 6A). As a result, this part of the domain is well sampled and documented by the crystals. However, we begin to lose information about the crystals that rapidly get funneled through the instability, because they are subject to heating and hence removal from the simulation (Fig. 6B). The crystals that travel through the spine to the tip of the instability are prone to alter the equilibrium state of the control volume at a given temperature and crystallinity (Fig. 6C-D). The tip of the instability is least sampled by the crystal population and has crystals with the shortest life span. While crystals in our simulations dissolve instantaneously, natural crystals exist for some time out of equilibrium even when they are in an instability like the one studied here. Hence our results show that there are two related, but distinct biases: On the one hand, crystal growth would not fully sample the instability. Crystals preferentially form at the tail of the instability (Fig. 6A) instead of at the tip (Fig. 6E) recording a biased record of dynamic environments within the flow system. On the other hand, crystal dissolution during disequilibration would dissolve certain growth rims and with it, their record of the magma dynamics.

7 Discussion

One of the fundamental problems in volcanology is to infer the complex magmatic processes occurring at depth prior to eruption from limited data. Crystals trapped in magma quenched upon eruption record at least some aspects of the pre-eruptive condition in the volcanic conduit directly (Demouchy & Mackwell, 2006; Spilliaert et al., 2006). However, leveraging crystal-scale data is difficult since most volcanic models are formulated at the system scale of hundreds of metres to tens of kilometers, and do not entail testable model predictions at the crystal scale that could be evaluated against this data. Here we identify and discuss the multiple indicators of the self-sustaining instability and the implications of our results.

7.1 Indicators

As stated previously (Cashman & Blundy, 2013; Kent & Cooper, 2018), many observations are non-unique indicators of dynamic processes; hence it is important to combine multiple different indicators to aid interpretation. In this section, we describe how the self-sustaining instability we have identified could be reflected in zonations, crystal chains, glomerocrysts, unstably distributed crystals, and cross-bedded crystal layers to facilitate testing of our model results against field data.

At the crystal scale, our simulations provide a new perspective on crystal zonations by associating them with crystal-driven convection. Researchers have previously invoked large scale thermal convection, (e.g. Singer et al., 1995; Bachmann et al., 2002; Huber et al., 2009; Murphy et al., 2000), mafic injections (Annen et al., 2005), and magma mixing (Sparks et al., 1977; Davidson & Tepley, 1997; Zellmer et al., 2003) to explain crystal zonations in natural samples. Our simulations demonstrate that zonations do not necessarily represent system-scale conditions, but may well capture thermal and flow-field heterogeneities at the crystalline scale. In the absence of a system scale overturn, processes like thermally- or bubble-driven flow, shearing (Bergantz et al., 2017), and deformation (Kennedy et al., 2008; Kahl et al., 2011) can all displace crystals into control vol-

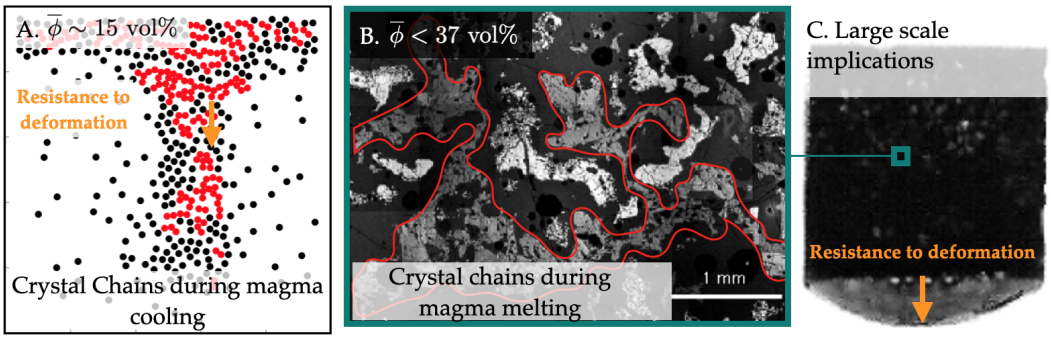

Figure 7. Crystal chains at low crystallinity. A is a snapshot of our simulation result as shown in Fig. 2C. The crystals in contact with neighboring crystals are colored red. There are horizontal and vertical crystal chains that form. Similar chains are found in the plagioclase crystals (in gray outlined in red of B) in the Holyoke Basalt Flow– originally published in Philpotts et al. (1998). C shows the experiment results from Philpotts et al. (1998). The hand sample data, of which B originated from, resists deformation when melted to have only 37 vol% crystallinity.

umes with different thermodynamic conditions and create zonations in the process. Depending on the size of the magma injection, its cooling and consequent termination of crystal displacement might take years allowing for sizable crystals to grow (Couch, 2003) and record local thermal heterogeneity. Our results suggest that crystal zonations for most crystals, especially fast forming crystals like plagioclase, are common, a prediction that is clearly borne out by observations (Shore & Fowler, 1996). Hence, for certain types of crystals, the absence of zonations could be a more valuable observational constraint than the presence of zonations, because there are fewer dynamic scenarios their absence would be compatible with.

In addition to zonations, one distinct observational signature of the self-sustaining instability we have identified is crystal chain formation. In Fig. 7A, we color crystals that are in less than half a radius proximity to other crystals in a single snapshot in red, highlighting the formation of transient crystal chains. These chains form due to crystals "swimming together", also known as crystal synneusis (Schwindinger & Anderson, Jr., 1989; Vogt, 1921), describing a fluid dynamic process commonly observed in Stokes flow (Lamb, 1911; Batchelor & Batchelor, 2000). In addition to this fluid dynamical process, crystals preferentially form near other crystals, because crystals partially transport the melt in which they formed and retain the thermodynamic conditions for crystallization. Although chains form in regions that are high in crystallinity, the average crystallinity in the entire domain is only 15 vol%.

Philpotts et al. (1998, 1999) observe the formation of crystal chains within the Holyoke Basaltic Magma Column, in some samples at no more than 25 vol% crystallinity (Philpotts et al., 1998, 1999) after having heated the samples (Fig. 7B). These crystals are intergrown and have "force chain" qualities, which means they transfer stress (Schleicher & Bergantz, 2017; Sun et al., 2010; Sandnes et al., 2011) and therefore aid resistance to deformation (Fig. 7C). In our simulation, we see a red lateral chain which appears to partially resist deformation in the vertical direction, suggesting that some of the crystals in our simulations act as force chains. Unlike Philpott et al., who observes crystal chains as the sample transitions from solid to melt-rich state, our simulations transition from melt- to solid-rich state. Contrary to the static inter-grown crystal chains in Philpott et al.'s experiments, our crystal chains are dynamic. In nature, the crystals that are in

contact for long enough may inter-grow appearing similar to the crystal chains seen in Philpott et al., 1998 (Fig. 7B). Force chains are observed in simulations at high crystal volume fractions (Bergantz et al., 2017) as well as in shear-induced flow simulations at low crystallinity (Qin & Suckale, 2020). Here, we interpret that force chains may also arise in crystal-driven convection at low crystallinity.

Another signature of a self-sustaining crystal convection instability closely related to crystal chains but morphologically distinct are glomerocrysts, which we define as non-elongated crystal clusters. Crystals in the self-sustaining instability transport the conditions in which they formed as clusters, creating a thermodynamic environment that is unique to the cluster (Culha et al., 2020). Although we do not model magma differentiation, our model suggests that secondary and tertiary crystals that form in the instability would show signatures of the residual melt, resembling the olivine, plagioclase, pyroxene, amphibole, and magnetite glomerocrysts in basaltic magma through magnetite fractionation (Garcia & Jacobson, 1979). Our model is also consistent with observations that suggest formation of glomerocrysts prior to complete crystallization of melt (Hogan, 1993). Since many of the crystals at the tip of the instability dissolve in our simulations (Fig. 6C-E), we would also expect resorption of crystals in glomerocrysts synchronous to glomerocrysts formation (Hogan, 1993).

Furthermore, our results suggest that the instability can transport crystals through the domain such that they are unstably stratified in the magmatic lens. Due to the temperature dependent thermodynamic conditions, the melt in the crystal rich cluster is colder and hence less dense (Fig. 1D&G) compared to the melt outside of the cluster. The dense crystal cluster of the self-sustaining instability drags the less dense melt in the crystal cluster downwards against its own relative buoyancy. Similarly, small crystals that are less dense than the average mixture within the instability may be brought along and deposited at the base of the domain with the rest of the dense crystals. Hence, the self-sustaining instability may explain observations such as the relatively less dense pyroxene and plagioclase crystals that are interstitial to denser chromite crystals in Stillwater outcrops (Jackson, 1961) and the rhythmic layering of light and dense crystals in Holyoke Basalt (Philpotts & Dickson, 2002).

Another indicator of the self-sustaining instability in a depositional environment could be cross-bedded crystal layering. As the crystal-rich cluster of the instability settles, the cluster deposits its crystals at the base of the magma lens. We do not model an entire lens, but in Fig. 5C, we show a snapshot of the instability with the purple crystals reaching the bottom of our simulation domain and the crystals spreading out. Unlike crystals individually "raining" through the magmatic lens, the rapid transport of crystals through multiple distinct clusters would suggest that cluster deposit crystals in a similar way as repeated gravity currents would. This process may be preserved as cross-bedded crystal layers, similar to observations at Duke Island, Skaergaard (Irvine, 1980) and Stillwater (Jackson, 1961) outcrops.

7.2 Implications

Our results suggest that local-scale heterogeneity can overprint broader system-scale trends, highlighting the challenge of deducing system-scale dynamics from individual crystals. For example, all of our simulations model a system-scale cooling of a hotter magma injection. At the crystal-scale, one would expect to see signatures of the system-scale cooling trend (similar to Fig. 6A), but instead, some of the crystals show consistent heating or partial heating zonations (Fig. 5D). The dynamic nature of the crystal-driven convection introduces spatial variations into the cooling history, such that crystals not only record temporal evolution but also a spatial heterogeneity. Our results suggest that quickly growing crystals would be able to sample more of the nuances associated with magma dynamics. Yet, with similarly fast rates of dissolution, these crystals are also more prone

to have their record erased. Fig. 4A and 6 quantify how many and characterize where the majority of the crystals dissolve in a self-sustaining instability simulation. This suggests that in natural samples, crystal zonation bands and entire crystals may dissolve due to dynamic disequilibration, erasing their record of a magmatic processes such as the self-sustaining instability during cooling (Fig. 6).

Since most of the crystals in the instability dissolve before they reach the simulation end (Fig. 4A and 6), the persisting sub-populations are biased towards suggesting the magma lens cooled much faster than it actually did. Underestimating the longevity of cooling has significant implications for interpreting magma storage timescales and temperatures. Recent literature on magma storage look at plagioclase and zircon crystals to understand timescales and temperatures of magma storage and notice surprisingly short timescales of magma storage in predominantly melt rich, or hot, conditions (Cooper & Kent, 2014; Rubin et al., 2017). Our results would suggest that crystal zonation records bias the interpretation of longevity of hot storage to be much shorter than it may actually be. Consequently, the time between mobilization of a magma body and eruption may be longer than the 100s of years the plagioclase crystals appear to indicate (Cooper & Kent, 2014). In terms of volcanic hazards, this could mean that magma reservoirs which have been stored as crystal-rich mushes may take longer to remobilize than previously thought. These model implications are consistent with the volcanic sites that stay active for multiple thousands of years contrary to the plagioclase crystal records (Gelman et al., 2013; Barboni et al., 2016) and research that argues that some crystals cannot resolve short lived processes (Kent & Cooper, 2018).

Another system-scale implication of our results is that convection at the crystal scale can enhance larger scale convective processes. The results from our previous work (Culha et al., 2020) suggest that crystal-driven convection may add to other convective processes such as thermal (Singer et al., 1995; Bachmann et al., 2002; Huber et al., 2009; Murphy et al., 2000) or bubble-driven convection (Bergantz et al., 2017) and can drive mesoscale flow. Our results here show that crystal settling becomes self-sustaining and faster when maintaining phase equilibrium. Phase change reactions could enhance other fluid dynamic instabilities by precipitating or dissolving crystals, similar to some of the concepts explored around double diffusive convection (Huppert & Turner, 1981; Huppert et al., 1983; Tait & Jaupart, 1989; Alsinan et al., 2017). For example, formation of denser-than-melt crystals in a sinking cold plume and cannibalism of crystals in a rising hot plume would accelerate thermal convection. Although our results show that the self-sustaining instability might be difficult to initiate in more felsic magmas (Fig. 3), formation and cannibalism of crystals in pre-conditioned convection will still occur and can enhance the convection. This dependence on a pre-conditioned convection for felsic magma has implications on speed of processes like compositional differentiation (Sparks et al., 1984; Culha et al., 2020). A further study of fluid and thermodynamic coupling with compositional differentiation may provide greater insight on global distribution of plutonic and volcanic compositions (Keller et al., 2015; Culha et al., 2020).

8 Conclusion

Our results quantify the thermal heterogeneity in crystal-scale data that will arise from phase change reactions in response to thermal disequilibration by dynamic flow. By resolving the crystal-melt interactions within a thermodynamically evolving crystal load, we identify a self-sustaining instability driven by crystallization within a cooling boundary layer. The crystals that travel in the cooling domain drag cool melt from the interface into hotter magma, altering the equilibrium state of the magma. A crystal cluster instability evolves and travels rapidly through the domain, resulting in a heterogeneous distribution of temperature, melt density, viscosity, and magma crystallinity. We find that the ratio of thermal diffusion speed and crystal advection speed will determine if the instability forms in natural systems. These conditions favor instability in basaltic

compositions at the sub-metre scale, where crystal and melt advection is faster than thermal diffusion.

The main contribution of our simulator is that it can track crystals and the thermal conditions that they sample, while allowing for crystal formation and dissolution. The crystal populations show a wide range of thermal zonations including heating, cooling, and oscillations, which resemble crystal zonations in natural samples. Moreover, we can keep record of the crystals that dissolve in our simulations, which make up the majority of the crystals in the self-sustaining instability. Hence, the crystal population left over from self-sustaining instability does not provide a complete record of the flow dynamics that have occurred in the system. Our work firmly emphasizes the significance of using multiple indicators in magmatic systems to decipher the processes creating the observable zonations in crystals.

Acknowledgments

The authors would like to thank Christy Till, Gail Mahood, Ayla Pamukcu and David Pollard for fruitful discussions throughout the development of the project. CC acknowledges support from the NSF's GRFP, Stanford University's McGee Grant and Stanford University's Lieberman Fellowship. TK acknowledges support from the Swiss National Science Foundation's Postdoc.Mobility Fellowship 177816. See our Github repository here for simulator: https://github.com/cculha4/Culha_Fluid_Therm.git.

References

Alasino, P. H., Ardill, K., Stanback, J., Paterson, S., Galindo, C., & Leopold, M. (2019). Magmatically folded and faulted schlieren zones formed by magma avalanching in the sonora pass intrusive suite, sierra nevada, california. *Geosphere*, *15*(5), 1677–1702.

Alsinan, A., Meiburg, E., & Garaud, P. (2017). A settling-driven instability in two-component , stably stratified fluids. , 243–267. doi: 10.1017/jfm.2017.94

Annen, C., Blundy, J., & Sparks, R. (2005). The genesis of intermediate and silicic magmas in deep crustal hot zones. *Journal of Petrology*, *47*(3), 505–539.

Bachmann, O., Dungan, M. A., & Lipman, P. W. (2002). The fish canyon magma body, san juan volcanic field, colorado: rejuvenation and eruption of an upper-crustal batholith. *Journal of Petrology*, *43*(8), 1469–1503.

Barbey, P., Gasquet, D., Pin, C., & Bourgeix, A. L. (2008). Igneous banding, schlieren and mafic enclaves in calc-alkaline granites: The Budduso pluton (Sardinia). *Lithos*, *104*(1-4), 147–163. doi: 10.1016/j.lithos.2007.12.004

Barboni, M., Boehnke, P., Schmitt, A. K., Harrison, T. M., Shane, P., Bouvier, A.-S., & Baumgartner, L. (2016). Warm storage for arc magmas. *Proceedings of the National Academy of Sciences*, *113*(49), 13959–13964.

Batchelor, C. K., & Batchelor, G. (2000). *An introduction to fluid dynamics*. Cambridge university press.

Bergantz, G. W., Schleicher, J. M., & Burgisser, A. (2017). On the kinematics and dynamics of crystal-rich systems. *Journal of Geophysical Research: Solid Earth*, *122*(8), 6131–6159.

Blundy, J., Cashman, K., & Humphreys, M. (2006). Magma heating by decompression-driven crystallization beneath andesite volcanoes. *Nature*, *443*(7107), 76–80.

Borisov, A. (2016). Mutual interaction of redox pairs in silicate melts: equilibria involving metallic phases. *Petrology*, *24*(2), 117–126. Retrieved from `http://link.springer.com/10.1134/S0869591116020028` doi: 10.1134/S0869591116020028

Borisov, A., & Behrens, H. (2013). The effect of titanium and phosphorus on ferric / ferrous ratio in silicate melts : an experimental study. *Contrib. Miner. Pet.*,

166, 1577–1591. doi: 10.1007/s00410-013-0943-9

Browne, B. L., Eichelberger, J. C., Patino, L. C., Vogel, T. A., Dehn, J., Uto, K., & Hoshizumi, H. (2006). Generation of Porphyritic and Equigranular mafic enclaves during magma recharge events at Unzen volcano, Japan. *J. Petrol.*, *47*(2), 301–328. doi: 10.1093/petrology/egi076

Cashman, K., & Blundy, J. (2013). Petrological cannibalism: the chemical and textural consequences of incremental magma body growth. *Contributions to Mineralogy and Petrology*, *166*(3), 703–729.

Cooper, K. M. (2019). Time scales and temperatures of crystal storage in magma reservoirs: Implications for magma reservoir dynamics. *Philosophical Transactions of the Royal Society A*, *377*(2139), 20180009.

Cooper, K. M., & Kent, A. J. (2014). Rapid remobilization of magmatic crystals kept in cold storage. *Nature*, *506*(7489), 480–483.

Costa, F., Shea, T., & Ubide, T. (2020). Diffusion chronometry and the timescales of magmatic processes. *Nature Reviews Earth & Environment*, 1–14.

Couch, S. (2003). Experimental investigation of crystallization kinetics in a haplogranite system. *American Mineralogist*, *88*(10), 1471–1485.

Culha, C., Suckale, J., Keller, T., & Qin, Z. (2020). Crystal fractionation by crystal-driven convection. *Geophysical Research Letters*, *47*(4), e2019GL086784. Retrieved from `https://agupubs.onlinelibrary.wiley.com/doi/abs/10.1029/2019GL086784` (e2019GL086784 10.1029/2019GL086784) doi: 10.1029/2019GL086784

Davidson, J. P., & Tepley, F. J. (1997). Recharge in volcanic systems: evidence from isotope profiles of phenocrysts. *Science*, *275*(5301), 826–829.

Demouchy, S., & Mackwell, S. (2006). Mechanisms of hydrogen incorporation and diffusion in iron-bearing olivine. *Phys. Chem. Miner.*, *33*(5), 347–355. doi: 10.1007/s00269-006-0081-2

Dupuy, C., Dostal, J., Girod, M., & Liotard, M. (1981). Origin of volcanic rocks from stromboli (italy). *Journal of Volcanology and Geothermal Research*, *10*(1-3), 49–65.

Flynn, L. P., & Mouginis-Mark, P. J. (1994). Temperature of an active lava channel from spectral measurements, kilauea volcano, hawaii. *Bulletin of Volcanology*, *56*(4), 297–301.

Garcia, M. O., & Jacobson, S. S. (1979). Crystal clots, amphibole fractionation and the evolution of calc-alkaline magmas. *Contributions to Mineralogy and Petrology*, *69*(4), 319–327.

Gelman, S. E., Gutiérrez, F. J., & Bachmann, O. (2013). On the longevity of large upper crustal silicic magma reservoirs. *Geology*, *41*(7), 759–762.

Ghiorso, M. S., & Gualda, G. A. R. (2015). An H_2O â CO_2 mixed fluid saturation model compatible with rhyolite â MELTS. *Contrib. to Mineral. Petrol.*, *169*(6), 1–30. doi: 10.1007/s00410-015-1141-8

Ginibre, C., Wörner, G., & Kronz, A. (2002). Minor-and trace-element zoning in plagioclase: implications for magma chamber processes at parinacota volcano, northern chile. *Contributions to Mineralogy and Petrology*, *143*(3), 300–315.

Ginibre, C., Wörner, G., & Kronz, A. (2007, 08). Crystal Zoning as an Archive for Magma Evolution. *Elements*, *3*(4), 261-266. Retrieved from `https://doi.org/10.2113/gselements.3.4.261` doi: 10.2113/gselements.3.4.261

Gualda, G. A. R., Ghiorso, M. S., Lemons, R. V., & Carley, T. L. (2012). Rhyolite-MELTS : a Modified Calibration of MELTS Optimized for Silica-rich, Fluid-bearing Magmatic Systems. *J. Petrol.*, *53*(5), 875–890. doi: 10.1093/petrology/egr080

Hogan, J. P. (1993). Monomineralic glomerocrysts: textural evidence for mineral resorption during crystallization of igneous rocks. *The Journal of geology*, *101*(4), 531–540.

Huber, C., Bachmann, O., & Manga, M. (2009). Homogenization processes in silicic

magma chambers by stirring and mushification (latent heat buffering). *Earth and Planetary Science Letters*, *283*(1-4), 38–47.

Huppert, H. E., Sparks, R., & Turner, J. S. (1983). Laboratory investigations of viscous effects in replenished magma chambers. *Earth and Planetary Science Letters*, *65*(2), 377–381.

Huppert, H. E., & Turner, J. S. (1981). Double-diffusive convection. *J. Fluid Mech.*. doi: 10.1017/S0022112081001614

Irvine, T. (1980). Magmatic density currents and cumulus processes. *American Journal of Science*, *280*(Jackson Volume), 1–58.

Jackson, E. (1961). Primary textures and mineral associations in the ultramafic zone of the stillwater complex, montana: Us geol. survey prof. paper 358, 106 p. 1963, chromium. *23rd Session, Sec*, *1*, 135–140.

Jayasuriya, K. D., OÊŒNeill, H. S., Berry, A. J., & Campbell, S. J. (2004). A Mössbauer study of the oxidation state of Fe in silicate melts. *Am. Mineral.*, *89*(1991), 1597–1609.

Kahl, M., Chakraborty, S., Costa, F., & Pompilio, M. (2011). Dynamic plumbing system beneath volcanoes revealed by kinetic modeling, and the connection to monitoring data: An example from mt. etna. *Earth and Planetary Science Letters*, *308*(1-2), 11–22.

Keller, C. B., Schoene, B., Barboni, M., Samperton, K., Husson, J. M., Hall, G., ... Angeles, L. (2015). Volcanic – plutonic parity and the differentiation of the continental crust. *Nature*, *523*, 301—-307.

Kennedy, B. M., Jellinek, A. M., & Stix, J. (2008). Coupled caldera subsidence and stirring inferred from analogue models. *Nature Geoscience*, *1*(6), 385–389.

Kent, A. J., & Cooper, K. M. (2018). How well do zircons record the thermal evolution of magmatic systems? *Geology*, *46*(2), 111–114.

Kojitani, H., & Akaogi, M. (1995). Measurement of heat of fusion of model basalt in the system diopside-forsterite-anorthite. *Geophysical research letters*, *22*(17), 2329–2332.

Kress, V. C., & Carmichael, I. S. E. (1991). The compressibility of silicate liquids containing Fe2O3 and the effect of composition, temperature, oxygen fugacity and pressure on their redox states. *Contrib. to Mineral. Petrol.*, *108*(1-2), 82–92. doi: 10.1007/BF00307328

Lamb, H. (1911). Xv. on the uniform motion of a sphere through a viscous fluid. *The London, Edinburgh, and Dublin Philosophical Magazine and Journal of Science*, *21*(121), 112–121.

Manga, M. (1996). Waves of bubbles in basaltic magmas and lavas. *J. Geophys. Res.*, *101*(B8), 17457. doi: 10.1029/96JB01504

Murata, K. (1970). Tholeiitic basalt magmatism of kilauea and mauna loa volcanoes of hawaii. *Naturwissenschaften*, *57*(3), 108–113.

Murphy, M., Sparks, R., Barclay, J., Carroll, M., & Brewer, T. (2000). Remobilization of andesite magma by intrusion of mafic magma at the soufriere hills volcano, montserrat, west indies. *Journal of petrology*, *41*(1), 21–42.

O'Neill, H. S. C., Berry, A. J., McCammon, C. C., Jayasuriya, K. D., Campbell, S. J., & Foran, G. (2006). An experimental determination of the effect of pressure on the Fe3/âFe ratio of an anhydrous silicate melt to 3.0 GPa. *Am. Mineral.*, *91*(2-3), 404–412. doi: 10.2138/am.2005.1929

Philpotts, A. R., Brustman, C. M., Shi, J., Carlson, W. D., & Denison, C. (1999). Plagioclase-chain networks in slowly cooled basaltic magma. *Am. Mineral.*, *84*(11-12), 1819–1829. doi: 10.2138/am-1999-11-1209

Philpotts, A. R., & Dickson, L. D. (2002). Millimeter-scale modal layering and the nature of the upper solidification zone in thick flood-basalt flows and other sheets of magma. *Journal of Structural Geology*, *24*(6-7), 1171–1177.

Philpotts, A. R., Shi, J., & Brustman, C. (1998). Role of plagioclase crystal chains in the differentiation of partly crystallized basaltic magma. *Nature*, *395*(6700),

343–346.

Qin, Z., Alison, K., & Suckale, J. (2019). Rotation matters-direct numerical simulations of rectangular particles in suspensions at low to intermediate solid fraction. *arXiv preprint arXiv:1903.08167*.

Qin, Z., & Suckale, J. (2016). A virtual laboratory for three-phase flow : 1 . Direct numerical simulations of bubble-crystal interactions in basaltic suspensions. , 1–60.

Qin, Z., & Suckale, J. (2017). Direct numerical simulations of gasâsolidâliquid interactions in dilute fluids. *Int. J. Multiph. Flow*, *96*(November), 34–47.

Qin, Z., & Suckale, J. (2020). Flow-to-sliding transition in crystal-bearing magma. *Journal of Geophysical Research: Solid Earth*, *125*(2), e2019JB018549.

Rae, A. S. P., Edmonds, M., Maclennan, J., Morgan, D., Houghton, B., Hartley, M. E., & Sides, I. (2016). Time scales of magma transport and mixing at K??lauea Volcano, Hawai'i. *Geology*, *44*(6), 463–466. doi: 10.1130/G37800.1

Rubin, A. E., Cooper, K. M., Till, C. B., Kent, A. J., Costa, F., Bose, M., ... Cole, J. (2017). Rapid cooling and cold storage in a silicic magma reservoir recorded in individual crystals. *Science*, *356*(6343), 1154–1156.

Ruth, D. C., Costa, F., de Maisonneuve, C. B., Franco, L., Cortés, J. A., & Calder, E. S. (2018). Crystal and melt inclusion timescales reveal the evolution of magma migration before eruption. *Nature communications*, *9*(1), 1–9.

Sack, R. O., Carmichael, I. S. E., Rivers, M., & Ghiorso, M. S. (1980). Contributions to mineralogy and petrology Ferric-Ferrous equilibria in natural silicate liquids at 1 bar. *Contrib. Miner. Pet.*, *75*, 369–376.

Sandnes, B., Flekkøy, E., Knudsen, H., Måløy, K., & See, H. (2011). Patterns and flow in frictional fluid dynamics. *Nature communications*, *2*(1), 1–8.

Santo, A. (2005). Magmatic evolution processes as recorded in plagioclase phenocrysts of nea kameni rocks (santorini volcano, greece). In M. Fytikas & G. E. Vougioukalakis (Eds.), *The south aegean active volcanic arc* (Vol. 7, p. 139 - 160). Elsevier. Retrieved from `http://www.sciencedirect.com/science/article/pii/S1871644X05800361` doi: https://doi.org/10.1016/S1871-644X(05)80036-1

Schleicher, J., & Bergantz, G. (2017). The mechanics and temporal evolution of an open-system magmatic intrusion into a crystal-rich magma. *Journal of Petrology*, *58*(6), 1059–1072.

Schwindinger, K. R., & Anderson, Jr., A. T. (1989). Synneusis of Kilauea Iki olivines. *Contrib. Miner. Pet.*, *103*, 187—-198.

Shane, P., & Smith, V. C. (2013). Using amphibole crystals to reconstruct magma storage temperatures and pressures for the post-caldera collapse volcanism at okataina volcano. *Lithos*, *156*, 159–170.

Shore, M., & Fowler, A. D. (1996). Oscillatory zoning in minerals; a common phenomenon. *The Canadian Mineralogist*, *34*(6), 1111–1126.

Singer, B. S., Dungan, M. A., & Layne, G. D. (1995). Textures and Sr, Ba, Mg, Fe, K, and Ti compositional profiles in volcanic plagioclase: Clues to the dynamics of calc-alkaline magma chambers. *Am. Mineral.*, *80*, 776–798.

Sparks, Huppert, H. E., & Turner, J. S. (1984). The fluid dynamics of evolving magma chambers. *Philosophical Transactions of the Royal Society of London. Series A, Mathematical and Physical Sciences*, *310*(1514), 511–534.

Sparks, Sigurdsson, H., & Wilson, L. (1977). Magma mixing: a mechanism for triggering acid explosive eruptions. *Nature*, *267*(5609), 315–318. Retrieved from `http://www.nature.com/nature/journal/v267/n5609/abs/267315a0.html{\%}5Cnpapers2://publication/uuid/1D841CE7-BD35-4AC5-8560-46844B6AF96B{\%}5Cnhttp://www.nature.com/doifinder/10.1038/267315a0` doi: 10.1038/267315a0

Spilliaert, N., Allard, P., Métrich, N., & Sobolev, A. (2006). Melt inclusion record of the conditions of ascent, degassing, and extrusion of volatile-rich alkali basalt

during the powerful 2002 flank eruption of mount etna (italy). *Journal of Geophysical Research: Solid Earth*, *111*(B4).

Suckale, J., Sethian, J., Yu, J., & Elkins-Tanton, L. (2012a). Crystals stirred up: 1. direct numerical simulations of crystal settling in nondilute magmatic suspensions. *Journal of Geophysical Research: Atmospheres*, *117*(8). doi: 10.1029/2012JE004066

Sun, Q., Jin, F., Liu, J., & Zhang, G. (2010). Understanding force chains in dense granular materials. *International Journal of Modern Physics B*, *24*(29), 5743–5759.

Tait, S., & Jaupart, C. (1989). Compositional convection in viscous melts. *Nature*, *338*(6216), 571–574. doi: 10.1038/338571a0

Till, C. B., Vazquez, J. A., & Boyce, J. W. (2015). Months between rejuvenation and volcanic eruption at yellowstone caldera, wyoming. *Geology*, *43*(8), 695–698.

Treiman, A. H. (1997). The parent magmas of the cumulate eucrites: A mass balance approach. *Meteoritics & Planetary Science*, *32*(2), 217–230.

Vance, J. A. (1962). Zoning in igneous plagioclase; normal and oscillatory zoning. *American Journal of Science*, *260*(10), 746–760.

Vogt, J. H. L. (1921). The physical chemistry of the crystallization and magmatic differentiation of igneous rocks. *The Journal of Geology*, *29*(4), 318–350.

Wallace, G. S., & Bergantz, G. W. (2005). Reconciling heterogeneity in crystal zoning data: An application of shared characteristic diagrams at Chaos Crags, Lassen Volcanic Center, California. *Contrib. to Mineral. Petrol.*. doi: 10.1007/s00410-004-0639-2

Whitney, J. A., & Stormer, J. C. (1985). Mineralogy, petrology, and magmatic conditions from the fish canyon tuff, central san juan volcanic field, colorado. *Journal of Petrology*, *26*(3), 726–762.

Zellmer, G., Sparks, R., Hawkesworth, C., & Wiedenbeck, M. (2003). Magma emplacement and remobilization timescales beneath montserrat: insights from sr and ba zonation in plagioclase phenocrysts. *Journal of Petrology*, *44*(8), 1413–1431.